



Milling performance of Inconel 718 based on DC short electric arc machining with graphite and W-Ag electrode materials

Zhouwei Liu¹ · Kai Liu² · Xiangyu Dai¹ · Jianping Zhou¹ · Yan Xu¹ · Zongjie Zhou¹

Received: 20 December 2021 / Accepted: 21 August 2022 / Published online: 1 September 2022
© The Author(s), under exclusive licence to Springer-Verlag London Ltd., part of Springer Nature 2022

Abstract

In order to solve the problems of poor dimensional accuracy, high-specific energy consumption (SEC), and poor surface integrity in DC short electric arc machining (SEAM), this paper proposes to use W-Ag alloy as the electrode material for machining nickel-based alloy (Inconel 718). Firstly, the effect of voltage and electrode material (graphite and W-Ag alloy) on the material removal rate (MRR), relative electrode wear rate (REWR), surface roughness (Sa), and SEC were investigated, and current and voltage during machining were measured by a multichannel data acquisition system. In addition, the surface morphology, cross section, and element distribution after machining were analyzed. The experimental results showed that W-Ag alloy as a tool electrode can obtain better performance in SEAM; its MRR reach 6314 mm³/min at 30 V which is twice as high as graphite electrode. The SEC of W-Ag alloy electrode is 32.64 kJ/cm³, significantly lower than that of graphite electrode with 84.16 kJ/cm³. The surface roughness is lower after machining with W-Ag alloy electrode, and the thermal damage layer is only half of that machined with graphite electrode.

Keywords Inconel 718 · Electrode with W-Ag · Short electric arc machining (SEAM) · Material removal rate (MRR) · Specific energy consumption (SEC) · Dimensional accuracy

1 Introduction

Nickel-based alloys, such as Inconel 718, are widely used in aerospace, petroleum, shipbuilding, and other industries because of their good high-temperature strength and excellent corrosion resistance. However, the traditional mechanical machining faces disadvantages such as low machining efficiency and high tool loss because of the high strength and high hardness characteristics of nickel-based alloys [1, 2]. Electric discharge machining (EDM) is an effective method for conductive and difficult-to-machine (DTM) materials and is suitable for machining nickel-based alloys [3]. However, the low machining

efficiency of conventional EDM has significantly limited its widespread application [4].

Electric arc machining (EAM), as a kind of EDM, has attracted the attention of many scholars for its higher machining efficiency. Meshcheriakov et al. [5] found that hydrodynamic forces in the gap could control the morphology of short arcs and proposed the arc dimensional machining (ADM), which achieved a higher MRR. Zhao et al. [6] proposed blasting erosion arc machining (BEAM) based on the hydrodynamic arc breaking mechanism and electrode with multiple holes, which significantly improve MRR in the processing of Inconel 718. Wang et al. [7] proposed compound machining by parallel arc and EDM power modules, which realize high MRR and low REWR. Han et al. [8, 9] proposed the high-speed EDM milling (H-SEAM) with moving electric arcs based on DC power supply, and the processing efficiency of H-SEAM was four times that of traditional EDM.

As a type of EAM, the voltage for SEAM is generally below 60 V, much lower than that in EDM. The current is typically between hundred and thousand amperes, much higher than that in EDM and other machining methods. SEAM has been an effective method for efficient machining

✉ Kai Liu
liuk_y@163.com

✉ Jianping Zhou
linkzhou@163.com

¹ School of Mechanical Engineering, Xinjiang University, Urumqi 830047, China

² Department of Mechanical and Energy Engineering, Southern University of Science and Technology, Shenzhen 518055, Guangdong, China

of DTM materials [10]. SEAM has achieved excellent performance in machining high hardness and toughness alloy parts such as cement rolls, aero-engine core unit casing, and honeycomb seals [11]. However, SEAM still faces several problems, including low MRR, large REWR, and high SEC; thus, a lot of effort has been made to work on these problems. Liu et al. [12] investigated the effect of electrode polarity on SEAM of titanium alloys found in the use of a DC power supply coupled with electrode negative machining can significantly improve MRR. Zhu et al. [13] studied the combined pulse voltage produced by the hybrid power system on SEAM performance found, and material removal rate (MRR) increases and tool wear rate (TWR) decreases with the increase of combined pulse voltage; however, the combined pulse voltage had a mild effect on surface roughness (Rz). In SEAM, the workpiece electrode is the anode, and the tool electrode is the cathode; both poles are discharged simultaneously to remove material from the workpiece. Different electrode materials have different melting and boiling points, electrical conductivity, and fugitive work; these physical characteristics influence current transfer rates, electrode loss, different dimensional accuracy, and roughness of the workpiece surface for SEAM machining [14]. Therefore, the choice of electrode material is particularly important; aluminum, steel, copper, graphite, and tungsten were usually used as tool electrodes [15]. The selection of electrode materials to increase the material removal rate and improve surface quality at the same time has become one of the key points in SEAM. Hua [16] experimented with W-Cu electrodes for EDM of TC4 and found that electrode losses increased with increasing peak current and pulse time and the decreasing pulse width. Li et al. [17] investigated the effect of different electrode materials on pulsed SEAM of GH4169 and found that graphite electrodes had lower loss rate, while copper electrodes had better surface quality. Zhou et al. [18] used copper, graphite, Q235 steel, and titanium as electrode materials to investigate the MRR of the SEAM and found that the graphite electrode had the most MRR and the lowest REWR, while the titanium electrode had the lowest SEC. Zhu et al. [19] conducted EDM DOE experiments, and machining Mo-Ti-Zr alloy with a 5- μm diameter tubular graphite electrode showed that MRR was most significantly influenced by peak current and had a clear interaction with pulse width and duty cycle. Kumar et al. [20] used copper, copper-chromium alloy, and copper-tungsten alloy to machine different types of titanium alloys (titanium alloy, Ti5Al-2.5Sn, and Ti-6Al-4 V) and finally used the Taguchi method to determine the optimum combination of parameters for minimum surface roughness; the effect of electrode material on surface roughness was found to be 4.38%.

W-Ag alloy is a metal sweating material composed of W and Ag [21]. W-Ag alloy is compatible with the advantages of W and Ag elements; it not only has the high melting

point, arc corrosion resistance, burnout resistance, and high hardness of W elements but also has the excellent electrical conductivity, thermal conductivity, and high plasticity of Ag elements. The use of W-Ag alloy electrode enables the lowest surface roughness to be achieved, resulting in very high precision in tools or other difficult machining parts [22]. In view of the good electrical conductivity, electron emission capacity, and wear resistance of W-Ag alloy in line with the principle of SEAM, this study uses W-Ag alloy as the tool electrode for the SEAM of Inconel 718.

In this paper, the machining performance under four different voltage conditions was compared by experiment. MRR, REWR, Sa, SEC, discharge waveform, workpiece surface, cross-sectional morphology, elemental distribution, and surface morphology of Inconel 718 machined with graphite and W-Ag alloy as electrodes were investigated.

2 Experiment details

2.1 Machine setup

As shown in Fig. 1, the SEAM equipment was composed of a self-developed short electric arc CNC milling machine tool, high-power supply, water pump, air compressor, and multichannel data acquisition systems. A high-power DC power supply, which had a maximum capacity of 30 V and 4000 A, was used to supply continuous energy to the manufacturing process. The electrode and workpiece were connected to the negative and positive poles of the power supply respectively. The CNC control cabinet controls the movement of the electrode along the Z-axis and the workpiece along the X-axis and Y-axis. The water pump and air compressor provide a high-speed water vapor mixture to flush the discharge gap. Finally, the combined action of the rotating electrode and the mixed dielectric makes the arc extinguishing and rapid removal of erosion for efficient machining. The multichannel data acquisition system was connected to a PC to record the voltage and current waveforms during machining and for further analysis.

2.2 Principle

The mechanism of material removal in the discharge channel is illustrated on Fig. 2, which mainly includes the processes such as reduction of the distance between electrode and workpiece, collision arc striking, arc diffusion, and arc movement. As shown in Fig. 2a, b, with the decrease of the distance between the electrode and the workpiece, tiny areas of the workpiece and the electrode surface collide first, thus establishing the initial conductive path of the discharge channel. As shown in

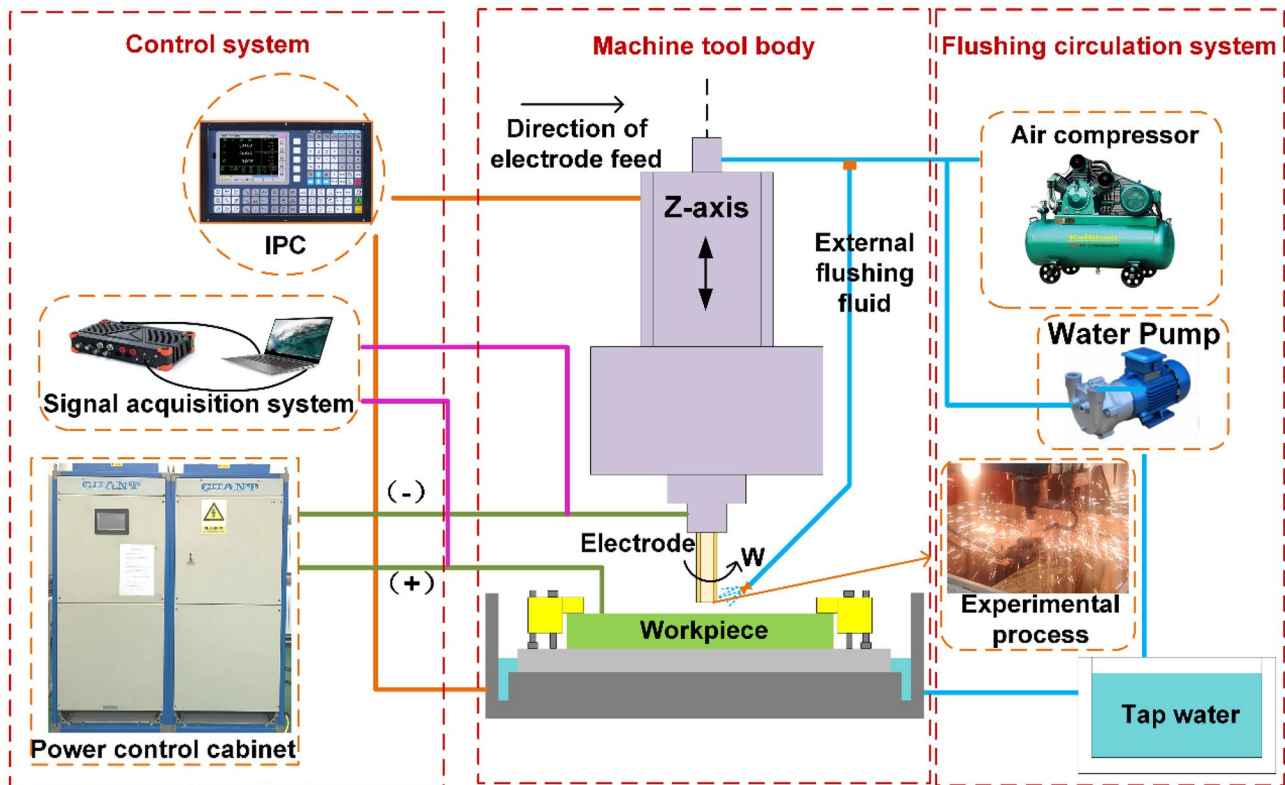


Fig. 1 Schematic of SEAM

Fig. 2c, d, the current is generated in the discharge circuit after the collision, and the contact resistance at the point of collision is high, so that the tiny area of collision generates massive Joule heat, causing the contact point to melt and vaporize to produce metal bridge and metal vapor, as shown in Fig. 2e, f. Subsequently, the discharge gap forms a stable arc due to thermal emission and field emission, and the diffusion of the discharge channel is achieved with the continuation of the current. Finally, many charged particles with high local temperature are generated, and the arc is generated by the breakdown of the field-assisted thermionic emission; the arc moves along the electrode feeding direction.

3 Experimental conditions and setup

3.1 Experimental conditions

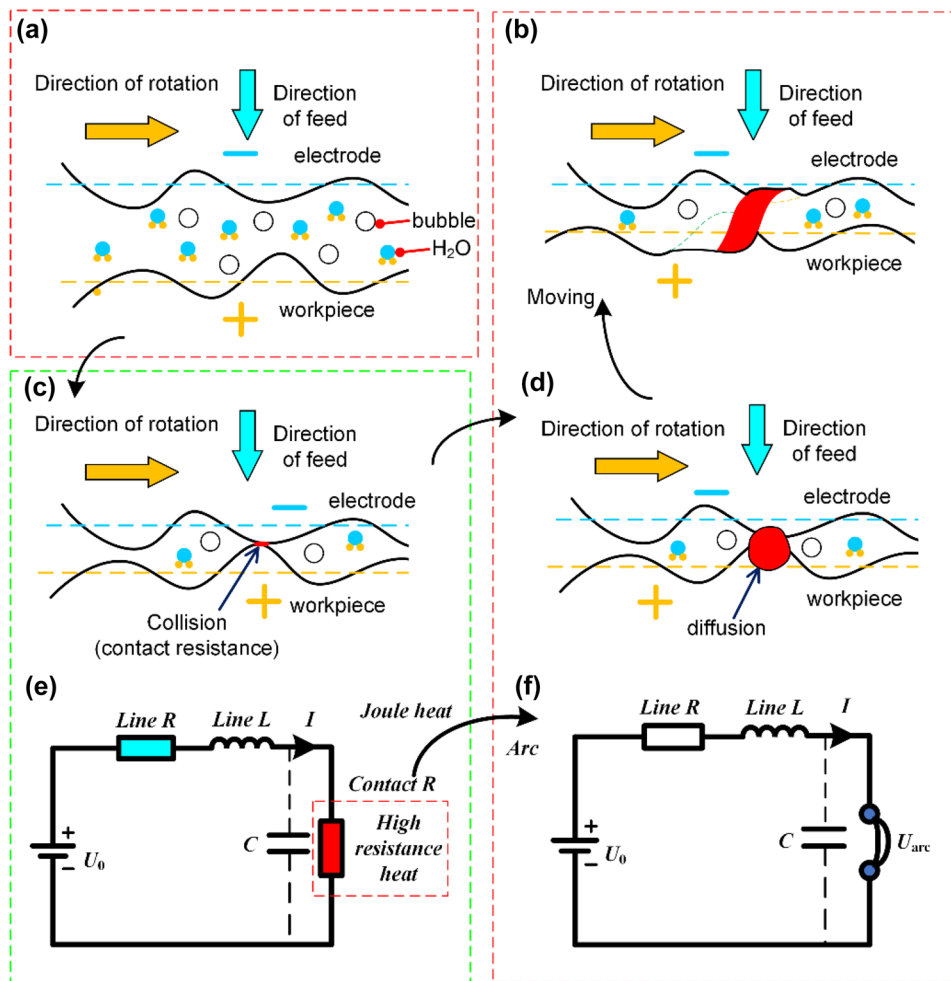
The electrodes are solid cylinders with a diameter of 5 mm, and the physical properties of the two electrode materials are shown in Table 1. The workpiece material is Inconel 718, a high-temperature nickel-based alloy, with a machining size of $30 \times 30 \times 10 \text{ mm}^3$. Inconel 718 is quite challenging because of the different chemical and mechanical properties of each phase [23].

Its chemical composition and mechanical properties are shown in Tables 2 and 3. A mixture of air and water was used as the dielectric for this study; air was supplied by an air compressor at a pressure of 0.3 MPa. A multi-data acquisition channel (DEWESoft SIRIUSi-HS-4xHV-4xLV, DEWESoft SIRIUSi-PWR-MCTS2 and HIE-C40-2000P5O15) was used to record the voltage and current. Its sample rate is set to 1 MHz. The digital microscope (VHX-6000) was used to analyze the surface roughness and 3D morphology of the machined samples. The machined workpieces were cut into $3 \times 3 \times 8 \text{ mm}^3$ specimens, which were inlaid, grinding, polishing, and chemically etched. Finally, the machined surfaces and cross section were visualized by scanning electron microscopy (SEM) for morphology, energy dispersive spectroscopy (EDS) for chemical elemental composition, and scanning confocal microscopy (SCM) for metallographic cross sections.

3.2 Experimental setup

The comparative experimental parameters are shown in Table 4. As negative polarity can achieve higher efficiency in SEAM, so this experiment was chosen to use negative polarity machining, and each parameter was repeated 3 times to ensure the accuracy of the experimental results. The MRR, REWR, and SEC are defined as follows:

Fig. 2 a, d, e, and f Discharge channel model in SEAM. c and d Equivalent circuit model



$$MRR = \frac{1000(M_{wi} - M_{wj})}{\rho_w t} (\text{mm}^3/\text{min}) \tag{1}$$

$$REWR = \frac{(M_{ei} - M_{ej})/\rho_e}{(M_{wi} - M_{wj})/\rho_w} \times 100\% \tag{2}$$

$$SEC = \frac{\rho_w \cdot \int_0^t (U(t) \times I(t)) dt}{(M_{wi} - M_{wj})} (\text{kJ}/\text{cm}^3) \tag{3}$$

M_{wi} and M_{wj} are the mass of the workpiece before and after machining (g), ρ_w is the density of the workpiece (g/cm^3), ρ_e is the density of the tool electrode, t is the machining time (min), M_{ei} and M_{ej} are the mass of the tool before and after machining (g), and $U(t)$ and $I(t)$ are the gap voltage and gap current collected in real time by the multichannel data acquisition system.

4 Results and discussions

4.1 Effect of electrode material on machining performance

Figure 3 shows the effect of electrode material on the performance of SEAM. The MRR of SEAM with W-Ag alloy electrode reached $6314 \text{ mm}^3/\text{min}$, which was nearly as twice as that of the graphite electrode. Since the metal ions inside W-Ag alloy electrode move more vigorously than at graphite electrode at high temperature and high current, more negatively charged particles enter the

Table 1 Physical properties of graphite and W-Ag

Electrode material	Graphite	W70Ag30
Density (g/cm^3)	1.85	14.9
Melting point ($^{\circ}\text{C}$)	3697	1083
Boiling point ($^{\circ}\text{C}$)	4830	2595
Heat conductivity ($\text{W}/(\text{m}\cdot\text{K})$)	129	396.4

Table 2 Chemical composition of Inconel 718 (%)

Element	%	Element	%	Element	%	Element	%
Al	0.2~0.8	Si	0.35	Cu	0.3	Mn	0.35
Mo	2.8~3.3	Nb	5.0~5.5	Cr	17~21	Ni	50~55
S	0.01	P	0.01	B	0~0.006	Nb	4.75~5.5
C	0.08	Ti	0.75~1.15	Co	1	Fe	Balanced

discharge channel per unit time at the negative electrode, resulting in a higher energy discharge process at W-Ag alloy electrode and a faster discharge of molten material, so the MRR significantly improved. However, the melting and boiling points of W-Ag alloy electrode are much lower than those of graphite electrode, and the partial melting of the W-Ag alloy electrode increases the electrode losses in the high temperature of SEAM. Therefore, the REWR of W-Ag alloy electrode is 5.26%, which is higher than that of graphite electrode at 4.12%. Considering the cost of experimental machining, we further explored the difference in electrode loss cost when machining with two different electrodes. It costs US \$2.31 per cubic centimeter for machining with graphite electrode and US \$15.32 per cubic centimeter for machining with W-Ag alloy electrode. When machining with W-Ag alloy electrode, the Sa is 99.24 μm, which is better than graphite electrode machining surface quality under the same conditions. The 3D profiles of Inconel 718 after machining are shown in Fig. 3b. The arc generated by the W-Ag alloy electrode has a larger and more concentrated discharge energy, which facilitates the realization of a better 3D profile. The SEC is 84.16 kJ/cm³ when machined with graphite electrode, and the SEC is only 32.64 kJ/cm³ when machined with W-Ag alloy electrode. Considering the experimental cost, we further calculated the electricity cost when machining two different electrodes. It costs US \$0.2338 per cubic centimeter when machined with graphite electrode and only US \$0.000783 when machined with W-Ag alloy electrode. Although the electrode cost is high when using W-Ag alloy electrode for SEAM, but it is less in power consumption, more effective, and more environmentally friendly.

4.2 Effect of voltage on the machining performance

The effect of voltage on MRR, RTWR, Sa, and SEC is shown in Fig. 4. As the voltage increases from 15 to 30 V,

Table 3 Physical and mechanical properties of Inconel 718

Microhardness	Melting point	Tensile strength	Yield strength	Elongation	Density
363 HBS	1260–1320 °C	965 MPa	550 MPa	30%	8.24 g/cm ³

the MRR of W-Ag alloy electrode and graphite electrode increases from 460 to 6314 mm³/min and 79 to 3231 mm³/min. As the voltage increases, the arc energy rises and becomes more stable, thus improving machining efficiency. However, as the voltage drops below 20 V, the process has difficulty maintaining a stable arc, thus becoming a weak arc and contact heat. Compared with graphite electrode, W-Ag alloy electrode has higher MRR at lower voltage and higher voltage. The REWR is higher when using small size electrodes without internal control than when machining with internal and external flushing [24]. When machining with both graphite and W-Ag alloy electrodes, the REWR decreases as the voltage increases. When the voltage is 15 V, the REWR of graphite electrode is 15.7%, while W-Ag alloy electrode is only 9.22%. However, when the voltage rises to 30 V, the REWR of graphite electrode is 4.12%, while the W-Ag alloy electrode is machined with the REWR of 5.26%. This is owing to the tendency towards a weak arc and contact heat at low voltage, and the mechanical strength of graphite electrode is much lower than that of W-Ag alloy. The melting and boiling points of graphite (3697 °C/4830 °C) are much higher than those of W-Ag alloy (1083 °C/2595 °C), and that is the reason for the low REWR obtained with graphite electrode. W-Ag alloy, as a typical sweat-cooled metal, is normally prepared by powder metallurgy. When using W-Ag alloy electrode for SEAM, the lower melting point of Ag first melts and evaporates and reduces the temperature in the cathode area of the arc, thus reducing the REWR. Another reason for the low REWR of W-Ag alloy electrode is due to the high heat conductivity of W-Ag alloy electrode. The heat is transferred to other places of W-Ag alloy electrode, so that the heat in the machining area is decreased, thus reducing the REWR of W-Ag alloy electrode. As shown in

Table 4 Parameters of SEAM

Parameters (unit)	Value
Tool polarity	Negative (–)
Voltage (V)	15, 20, 25, 30
Flushing pressure (MPa)	0.3
Liquid flow (L/min)	2
Milling depth (mm)	2
Electrode rotation speed (rpm)	600
Electrode material	W70Ag30, graphite
Workpiece material	Inconel 718

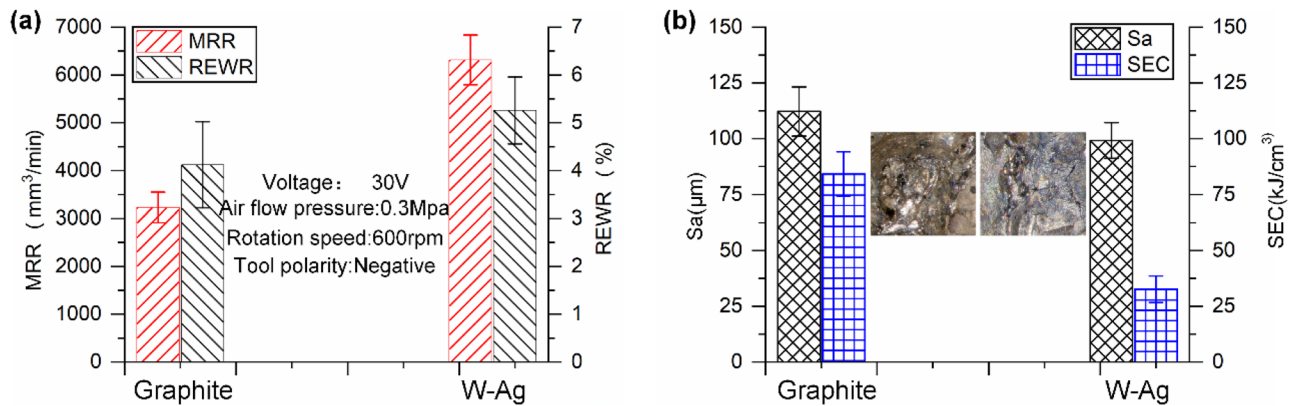


Fig. 3 Effect of electrode material on machining performance

Fig. 4, the Sa gradually increases as the voltage rises from 15 to 30 V. At a voltage of 30 V, when machining with graphite electrode, Sa is 112.21 μm, and when using W-Ag alloy electrode, Sa is 99.24 μm. W-Ag alloy electrode has low thermal conductivity and heat dissipation properties; the temperature of the arc machining area drops rapidly after machining, which facilitates the achievement of better surface quality. Figure 4b also shows the effect of voltage on the SEC for the two electrodes, the SEC of graphite electrode was 84.16 kJ/cm³, while the SEC of W-Ag alloy electrode was 32.64 kJ/cm³. This is mainly because of the fact that the graphite electrode processes with a peak current of 469 A, while the W-Ag alloy electrode has a higher peak discharge current of 839 A. The W-Ag alloy electrode can produce a stronger arc energy in a short period of time. Due to the high-current and high-energy nature of the W-Ag alloy electrode leads to a greater concentration of energy, the heat of the arc acting on the W-Ag alloy electrode will spread more easily, and the proportion of arc energy consumed will be less, thus reducing the SEC.

4.3 Voltage and current characteristics analysis

This study is based on the DC power supply, the current can directly determine the arc discharge power, and the peak current represents the instantaneous maximum energy output. Figure 5a, b shows the voltage and current waveforms during SEAM. As the collision between the electrode and the workpiece draws arc, a significant voltage drop can be seen in the waveform. There are significant differences in the waveforms during machining due to the different electron emission capabilities of the two materials. Figure 5a shows the voltage-current waveform of the graphite electrode in SEAM. The peak current of the graphite electrode is 469.1 A, and the discharge process is continuous. This is mainly because of the graphite electrode with low losses and high melting and boiling point, so the electrode melts very little at the high temperature of the SEAM, and there is no short circuit because of secondary discharge. Figure 5b shows the voltage-current waveform of the W-Ag alloy electrode. Because of the different electron escape works of the two

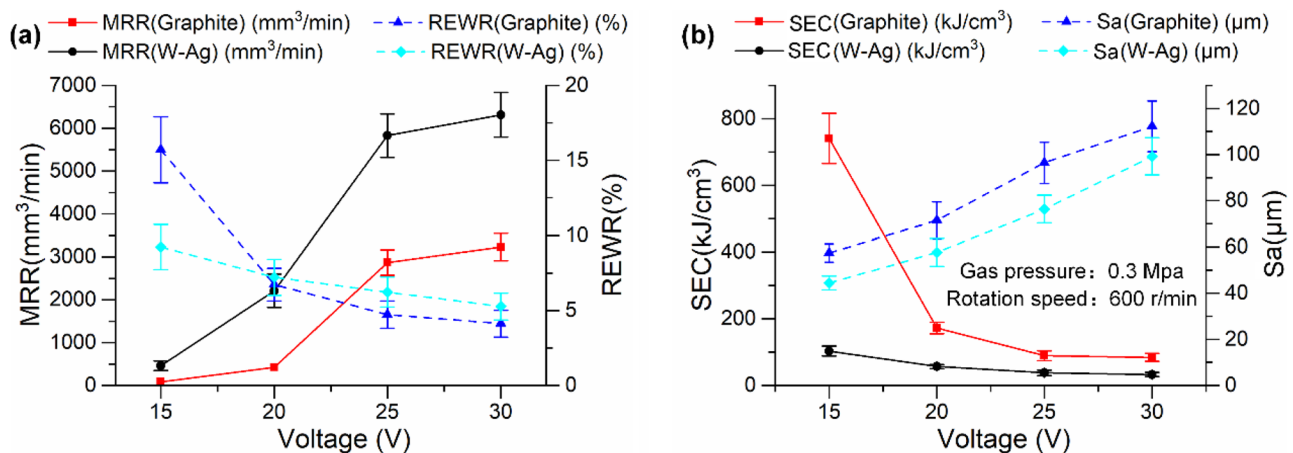


Fig. 4 Effect of voltage on machining performance. **a** Graphite. **b** W-Ag

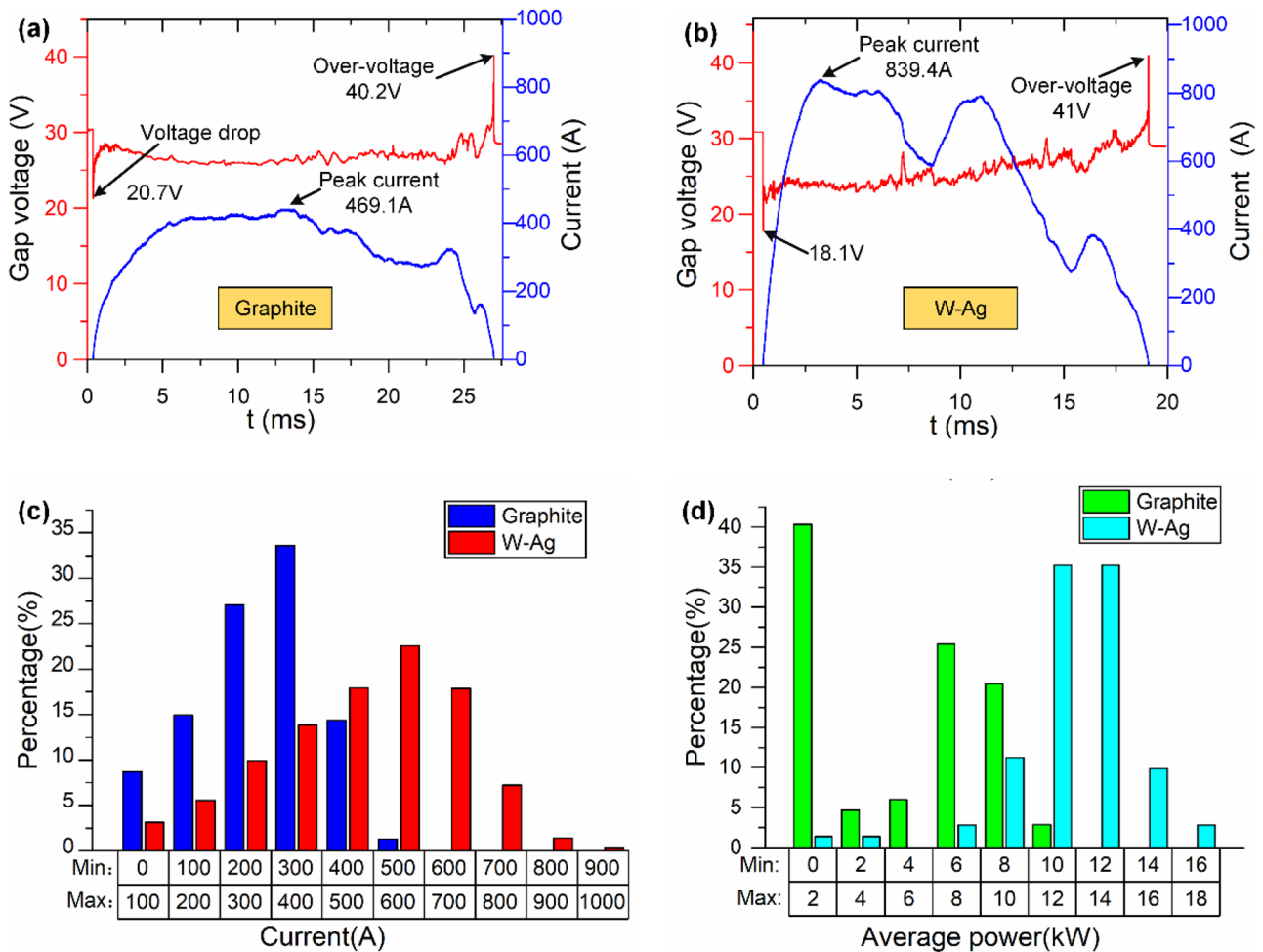


Fig. 5 a Waveforms with graphite. b Waveforms with W-Ag. c Current distribution. d Average power distribution

materials, more electrons are generated when machining with W-Ag alloy electrode at the same time, more electrons pass through the liquid metal bridge, higher energy is generated, and the discharge current is higher. As a metal, the oxide layer of the W-Ag alloy, has a strong electron-emitting capacity and a higher heat dissipation capacity than graphite, so it has a higher discharge current (peak current of 839.4 A). Therefore, when W-Ag alloy is used as electrode material for SEAM, the power utilization is greatly improved, and the energy of the arc is greater.

To investigate the energy distribution between graphite electrode and W-Ag alloy electrode during SEAM, the currents during machining were counted at time intervals. As shown in Fig. 5c, because of the different conductivity and heat dissipation of the two electrode materials, the energy distribution of the two materials during machining is different. The percentage of graphite electrode and W-Ag alloy electrode machining process current in the range 0–600 A is 100% and 73%. When the current stops increasing further, the heat generated by the arc reaches a state

of thermodynamic equilibrium under the combined effect of the working medium and the rotation of the electrodes; at this point, the current fluctuates within a narrow range and reaches a relatively stable value. The machining current is mostly concentrated around 400 A when graphite is used as the electrode, while the machining current is mostly concentrated at 600 A when W-Ag alloy is used as the electrode. During the machining of W-Ag alloy electrode, it has more energy and more consistent current distribution than the machining with graphite electrode. Because of the greater energy generated when machining with W-Ag alloy electrodes, debris can be discharged in time, resulting in a more continuous discharge process, longer duration, and more consistent current distribution. The average power for SEAM using both electrodes is shown in Fig. 5d. With the increase of power output energy, the energy of the plasma discharge channel between the two poles also increases. The average power is mostly in the range of 0–2 kW for graphite electrode and 1.2–1.6 kW for W-Ag alloy electrode. This is due to the higher current density of the W-Ag alloy electrode

in the discharge channel of the SEAM resulting in higher arc energy, and the average power throughout the process is much higher than that of the graphite electrode.

4.4 Analysis of dimensional accuracy and roughness

The effect of different electrode materials on the quality and accuracy of machining Inconel 718 is shown in Fig. 6. As shown in Fig. 6a, b, when graphite is used as an electrode, it has higher surface overcut, and the workpiece has poorer surface integrity than that of the W-Ag alloy electrode, so the surface shape of W-Ag alloy electrode is better. The 3D profile of the workpiece surface after machining with W-Ag alloy electrode and graphite electrode is shown in Fig. 6c, d. The highest value after machining with graphite electrode is 5006.409 μm , while W-Ag alloy electrode is only 4201.048 μm ; this means the surface machined with W-Ag alloy electrode is more quality. The W-Ag alloy electrode has low thermal conductivity and heat dissipation properties, and the temperature of the arc machining area drops rapidly after machining, so it is conducive to achieving better surface roughness for surface machining. Figure 6e shows a comparison of the ideal machined profile and the actual machined profile line for two electrode materials. The contour line of graphite electrode is far from the ideal machining contour line; the contour line of W-Ag alloy electrode is close to the ideal inverse contour line. The arc discharge energy of the W-Ag alloy electrode is more concentrated, the thermal conductivity and heat dissipation of the electrode are better, so the arc area dissipates quickly after machining is conducive to improving the three-dimensional profile and roughness of the surface. The distance between the ideal contour and the lowest point of machined was measured by taking 20 contour lines at a unit of 1 μm spacing on the machined surface of W-Ag alloy electrode and graphite electrode respectively, and the responding radar map was shown in Fig. 6f. As shown in the Fig. 6f, the overcut of graphite electrode is significantly larger than that of W-Ag alloy electrode, so the machining dimensional accuracy of W-Ag alloy electrode is better. That is mainly because the W-Ag alloy electrode increases the speed of charged particle movement in the discharge channel, accelerates chip discharge, and makes the discharge process more uniform, thus improving dimensional accuracy. The excellent dimensional accuracy of W-Ag alloy electrodes provides a better basis for subsequent finishing.

4.5 Surface topography and formation mechanism

Figure 7 shows the SEM images of machined surface of Inconel 718 for SEAM. Evidently, there are different degrees of droplets, hollows, erosion holes, micro-cracks, re-solidified layers, and other microstructures distributed unevenly on the surfaces

of the specimens prepared using both material electrodes, as shown in Fig. 7a, b. The droplets represent the metal vapor frozen in the interstices of the surface as the media cools. The discharge process removes the material by means of a high-speed arc, thus creating a hollow. Erosion holes are formed on the surface of the workpiece by gases precipitated during the melting process. The dramatic change in temperature between the heat-affected zone and the base material leads to irregular stress changes and stresses exceeding the ultimate tensile strength of the material, forming micro-cracks. The rapid cooling of the medium allows the molten material to resolidify on the surface of the workpiece, thus forming re-solidified layers. As seen in Fig. 7a, c, under the same machining conditions, the surface of the workpiece machined with W-Ag alloy electrode appears partially smooth coating, without obvious cracks, with small droplets and few air hollows. However, in the graphite electrode machining workpiece surface, as shown in Fig. 7b, the surface has obvious micro-cracks with re-solidified layers, and the galvanic corrosion products are difficult to discharge in the discharge area, affecting the machining stability. At the high-power discharge output of the DC power supply, the number and area of graphite electrode re-solidified layers are significantly more than that of W-Ag alloy electrode, as shown in Fig. 7b, d. It can be inferred that the use of W-Ag alloy electrode leads to smaller and more uniformly distributed erosion particles and improves the stability of SEAM.

4.6 EDS analysis of the workpiece surface

After the completion of the SEAM process, EDS tests on explosive and molten surface were performed to investigate elemental changes, and the results are presented in Fig. 8. The corresponding elemental content of the base material is shown in Table 2. As shown in Table 2 and Fig. 8a, the C-element content of machining with graphite electrode is greatly increased. This is because graphite contains a large amount of element C, which is partially transferred from the graphite electrode to the workpiece surface under the effect of high-speed rotation of the electrode. The element Ni in the workpiece decomposes and oxidizes at high temperatures to form NiO, so the content of the element O increases. As shown in Fig. 8b, when using W-Ag alloy electrode, the surface of the workpiece appears Ag and W elements. This is due to the precipitation of Ag from W-Ag alloy electrode at the high temperature and heat of arc machining, which adheres to the workpiece surface and verifies that the use of W-Ag alloy electrode in Fig. 6e results in a better surface quality with a profile closer to the ideal machining line. As shown in Fig. 8, the W-Ag alloy electrode has a higher proportion of nickel elements after machining; this is due to the proportion of nickel elements increases with the increase of electrical conductivity, and the W-Ag alloy electrode has better electrical conductivity compared with graphite electrode.

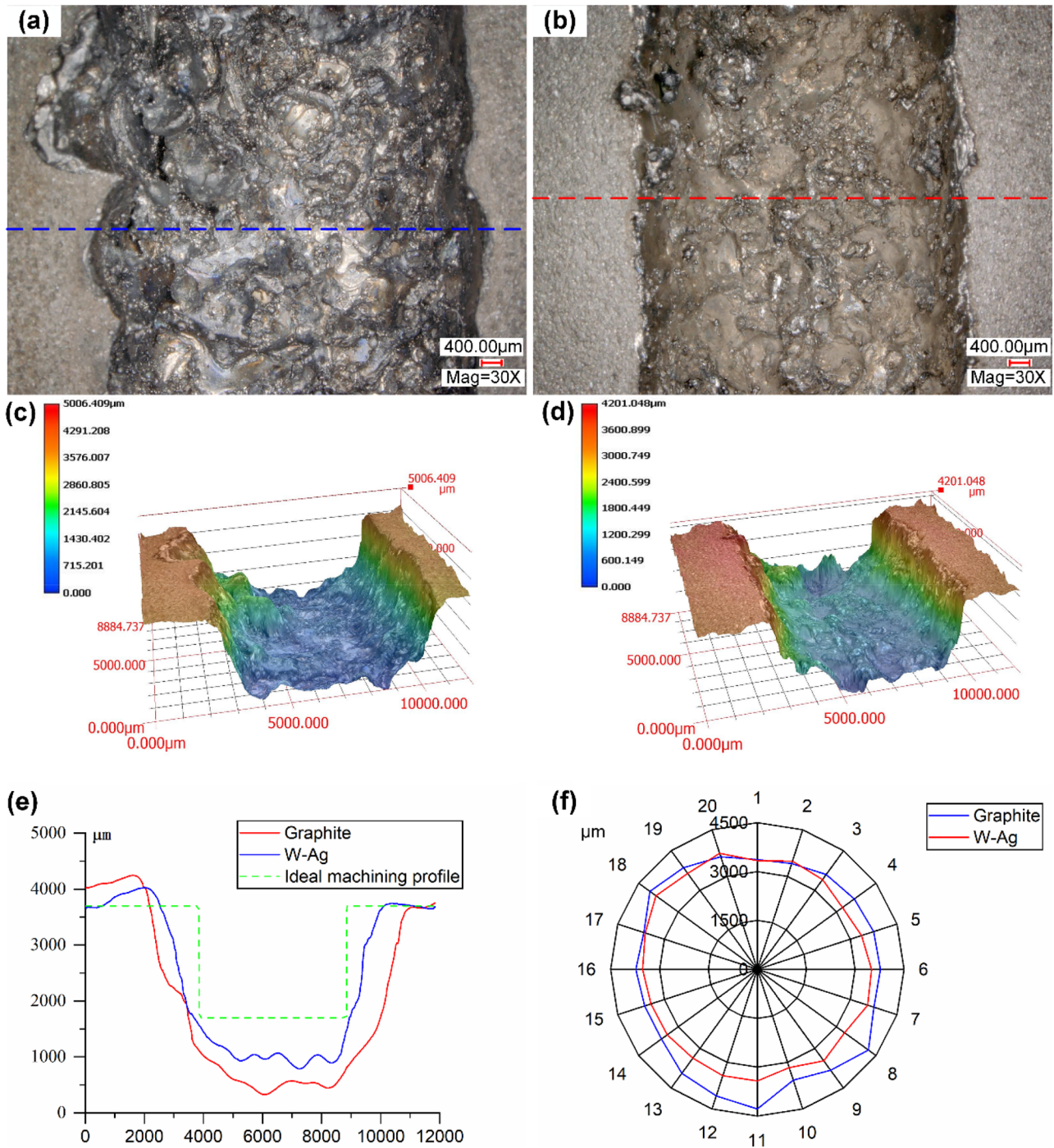


Fig. 6 a Surface profile of graphite. b Surface profile of W-Ag. c 3D surface topographies of graphite. d 3D surface topographies of W-Ag. e Contour profile comparison. f Comparison of depth overcuts

4.7 Cross-section analysis

To further investigate the process characteristics of SEAM with different materials, Inconel 718 samples machined at 30 V to explore the cross-sectional morphology. The cross-sectional metallographic profiles and the elemental

composition of the thermal damage layer of the workpiece machined with different electrode materials are shown in Fig. 9. The thermal damage layer and base material can be clearly seen in Fig. 9a, b, and the cross sections of the two materials are very different after machining. In addition, microcracks can be found on the surface of the workpiece

Fig. 7 Effect of different electrode materials on the surface morphology of the workpiece. **a** and **b** Graphite. **c** and **d** W-Ag

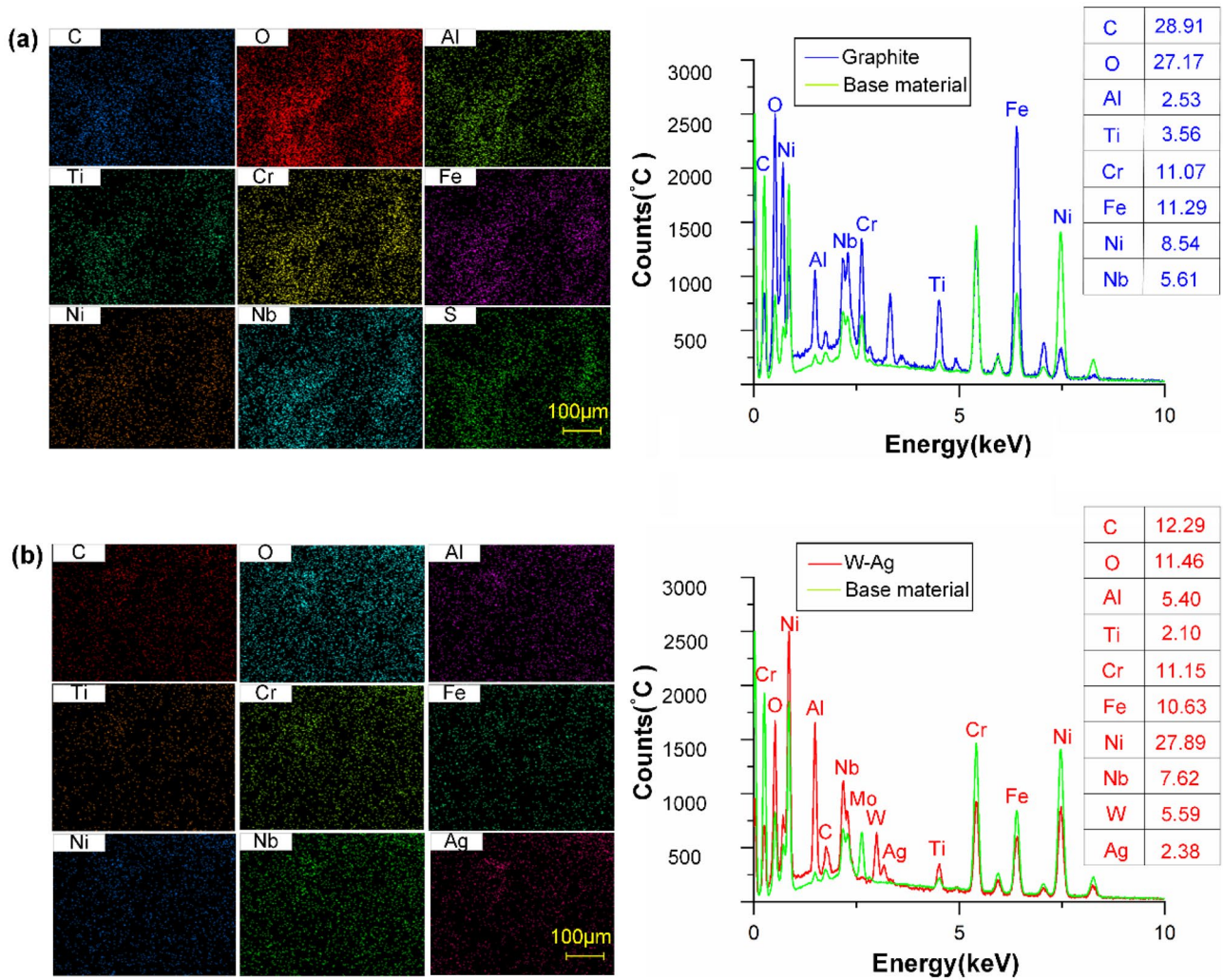
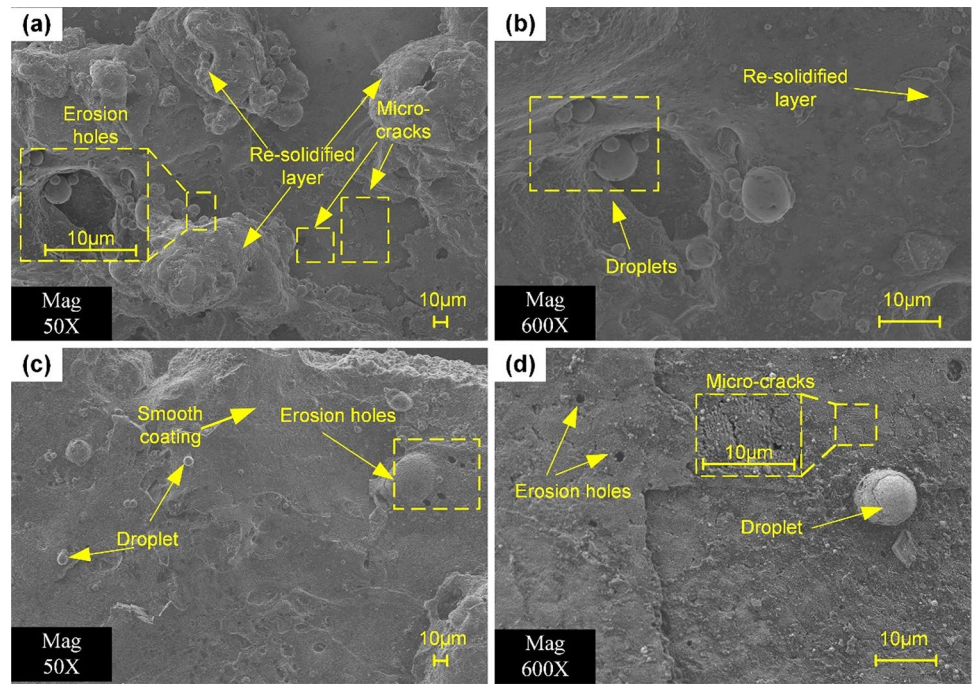


Fig. 8 EDS spectrum of SEAM. **a** Graphite. **b** W-Ag

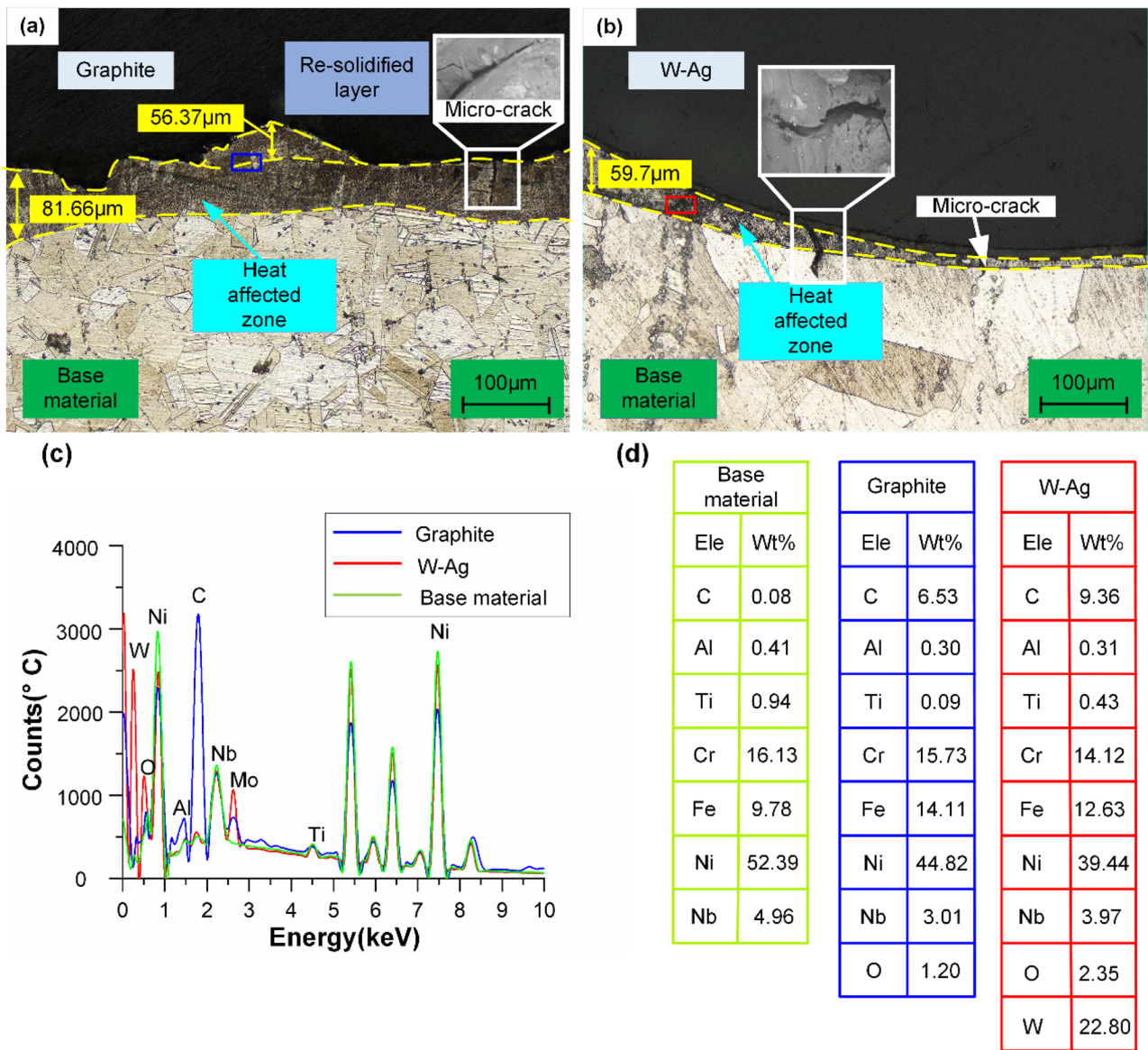


Fig. 9 Cross-sectional SCM image of Inconel 718. **a** Graphite. **b** W-Ag. **c** EDS spectra of workpieces. **d** Percentage of elements

due to stress concentrations exceeding the ultimate tensile strength of Inconel 718. Figure 9a shows the cross-sectional morphology machined with a graphite electrode. The thickness of thermal damage layer is 138.03 μm in total, including the re-solidified layer of 56.37 μm and the heat-affected zone of 81.66 μm. Figure 9c shows that the graphite electrode machining after the thermal damage layer in the C-element content increased sharply, in line with Fig. 8 workpiece surface element comparison results. Graphite electrode in the high-temperature, high-speed rotation of the process to produce wear, part of the graphite particles, and workpiece surface etching material solidified together, forming re-solidified layer, so the C element is obviously higher in the surface content; as

the electrode relative wear reduced, the workpiece on the C-element content also reduced. When W-Ag alloy is used as the electrode, the thickness of the heat-affected zone of the workpiece is 59.7 μm, as shown in Fig. 9b. Because W-Ag alloy is a metallic material with higher arc energy and faster material removal than graphite, the etchings flake directly from the workpiece under the strong impact of the moving arc before they spoilage, so the thermal damage layer machined with W-Ag alloy electrode is only half of that with graphite electrode. A comparison of the thermal damage layer and the base material elements of Inconel 718 machined with the W-Ag alloy electrode is shown in Fig. 9c, d; W appears in the thermal damage layer for the same reason as the appearance of element C

after graphite electrode machining. C and O carbonize and oxidize the thermal damage layer, producing NiC and NiO, two types of brittle material that also make some micro-cracks appear in the cross-sectional morphology.

5 Conclusions

This paper investigates the milling performance of graphite electrode and W-Ag alloy electrode materials for SEAM with DC of Inconel 718. The effects of tool-electrode materials and voltage on the MRR, REWR, SEC, and surface roughness were studied. Moreover, the V-A waveform, dimensional accuracy, surface morphology, elemental distribution, and cross-section morphology of the workpiece were examined. The main conclusions are as follows:

1. By observing the inter-pole voltage and current waveforms, the W-Ag alloy electrode could achieve larger currents, resulting in higher MRR and uniform workpiece surface after machining.
2. As the voltage decreased, MRR was gradually decreased, RTWR and SEC were increased, and the surface quality was improved.
3. The maximum MRR of the W-Ag alloy electrode was 6314 mm³/min, which was twice as high as that of the graphite electrode. The SEC of W-Ag alloy electrode was only 32.64 kJ/cm³, less than half that of graphite electrode. The W-Ag alloy electrode had much lower surface roughness than graphite electrode.
4. Droplets, hollows, erosion holes, micro-cracks, re-solidified layers, and other microstructures were observed on the micro-surface after SEAM. With W-Ag alloy electrode, the etchant particles were smaller and more evenly distributed, which improved the stability of SEAM, and its performance was significantly improved.
5. The EDS analysis showed that there was a chemical reaction between the workpiece material, the tool material, and dielectric. The machined surface significantly increased the O and the elements of the tool electrode (C or W-Ag).
6. Different electrode materials resulted in different cross sections after machining. The thermal damage layer of Inconel 718 machined with W-Ag alloy electrode is only half of that machined with graphite electrode.

Author contribution Zhouwei Liu, data curation and writing—original draft preparation. Kai Liu, conceptualization and methodology. Xiangyu Dai, experimental planning. Jianping Zhou, reviewing and editing. Yan Xu, investigation and validation. Zongjie Zhou, data processing.

Funding This research was supported by the Natural Science Foundation of China (Grant No. 51765063), the Key Research

and Development Projects in the Autonomous Region (Grant No. 2018B02009-1), and Xinjiang Uighur Autonomous Region Talent Project (Grant No. 10020000204).

Data availability All data generated or analyzed during this study are included in this published article.

Declarations

Conflict of interest The authors declare no competing interests.

References

1. Mishra V, Pandey PM (2018) Experimental investigations into electric discharge grinding and ultrasonic vibration-assisted electric discharge grinding of Inconel 601. *Mater Manuf Process* 33:1518–1530. <https://doi.org/10.1080/10426914.2018.1453143>
2. Jeyaprakash N, Yang CH (2020) Comparative study of NiCrFeMoNb/FeCrMoVC laser cladding process on nickel-based superalloy. *Mater Manuf Process* 35:1383–1391. <https://doi.org/10.1080/10426914.2020.1779933>
3. Li C, Xu M, Yu Z, Huang L, Li S, Li P, Niu Q (2020) Electrical discharge-assisted milling for machining titanium alloy. *J Mater Process Technol* 285:116785. <https://doi.org/10.1016/j.jmatprotec.2020.116785>
4. Venkatalaxmi A, Padmavathi BS, Amaranath T (2004) A general solution of unsteady Stokes equations. *Fluid Dyn Res* 35:329–336. <https://doi.org/10.1016/j.fluidyn.2004.03.001>
5. Meshcheriakov G, Nosulenko V, Meshcheriakov N, Bokov V (1988) Physical and technological control of arc dimensional machining. *CIRP Ann - Manuf Technol* 37:209–212. [https://doi.org/10.1016/S0007-8506\(07\)61619-9](https://doi.org/10.1016/S0007-8506(07)61619-9)
6. Zhao W, Gu L, Xu H, Li L, Xiang X (2013) A novel high efficiency electrical erosion process - blasting erosion arc machining. *Procedia CIRP* 6:621–625. <https://doi.org/10.1016/j.procir.2013.03.057>
7. Wang F, Liu Y, Zhang Y, Tang Z, Ji R, Zheng C (2014) Compound machining of titanium alloy by super high speed EDM milling and arc machining. *J Mater Process Technol* 214:531–538. <https://doi.org/10.1016/j.jmatprotec.2013.10.015>
8. Han F, Wang Y, Zhou M (2009) High-speed EDM milling with moving electric arcs. *Int J Mach Tools Manuf* 49:20–24. <https://doi.org/10.1016/j.ijmachtools.2008.08.005>
9. Kou Z, Han F (2018) On sustainable manufacturing titanium alloy by high-speed EDM milling with moving electric arcs while using water-based dielectric. *J Clean Prod* 189:78–87. <https://doi.org/10.1016/j.jclepro.2018.04.072>
10. Liang C, Zhou J, Zhu Z (2007) Study and application of short arc large current working technology. *Modern Manuf Eng* 12:92–93
11. Zhou J, Liang C, Teng W (2008) Study on rules in material removal rate and surface quality of short electric arc machining process. *Adv Mater Res* 33(5):1313–1318
12. Liu K, Zhou J, Zhou Z, Xu Y, Hu G, Zhang L, Song D (2020) Milling performance of titanium alloy based on short electric arc machining with direct current power source. *Int J Adv Manuf Technol* 110:1641–1652. <https://doi.org/10.1007/s00170-020-05937-z>
13. Zhu G, Zhang Q, Wang H, Wang K, Zhang M (2017) Machining behaviors of short electrical arc milling with high frequency and high voltage pulses. *Int J Adv Manuf Technol* 90:1067–1074. <https://doi.org/10.1007/s00170-016-9399-1>
14. Chung DK, Shin HS, Park MS, Kin BH, Chu CN (2011) Recent researches in micro electrical machining. *Int J Precis Eng Manuf* 12:371–380. <https://doi.org/10.1007/s12541-011-0049-0>

15. Lee SH, Li XP (2001) Study of the effect of machining parameters on the machining characteristics in electrical discharge machining of tungsten carbide. *J Mater Process Technol* 115:344–358. [https://doi.org/10.1016/S0924-0136\(01\)00992-X](https://doi.org/10.1016/S0924-0136(01)00992-X)
16. Hua Q (2014) Experiment on complicated cavity of titanium alloy 545 by EDM. *J Southwest China Normal Univ (Nat Sci Ed)* 9:138–140
17. Li XZ, Zhou JP, Wang KD, Xu Y, Wu TB (2019) Experimental research on machinability of different electrode materials for SEAM of the nickel-based superalloy GH4169. *Proc Inst Mech Eng C J Mech Eng Sci* 232(24):4528–4537. <https://doi.org/10.1177/0954406218755184>
18. Zhou Z, Liu K, Xu Y, Zhou J, Wang L (2021) Experimental study on high-efficiency DC short electric arc milling of titanium alloy Ti6Al4V. *Int J Adv Manuf Technol* 117:2775–2789. <https://doi.org/10.1007/s00170-021-07864-z>
19. Zhu Y, Gao F, Sun C, Niu L, Gu L (2016) Experimental study of electrical discharge machining for TZM. *Aeronaut Manuf Technol* 14:61–64
20. Kumar S, Batish A, Singh R, Singh TP (2014) A hybrid Taguchi-artificial neural network approach to predict surface roughness during electric discharge machining of titanium alloys. *J Mech Sci Technol* 28:2831–2844. <https://doi.org/10.1007/s12206-014-0637-x>
21. Azar GTP, Rezaie HR, Gohari B, Razavizadeh H (2013) Synthesis and densification of W-Cu, W-Cu-Ag and W-Ag composite powders via a chemical precipitation method. *J Alloys Compd* 574:432–436. <https://doi.org/10.1016/j.jallcom.2013.04.172>
22. Qureshi AH, Azhar SM, Hussain N (2010) The effect of cobalt addition on sintering and microstructural behaviour of silver-tungsten (Ag-W) composite. *J Therm Anal Calorim* 99:203–209. <https://doi.org/10.1007/s10973-009-0152-y>
23. Ajmal KM, Yi R, Zhan Z, Ji J, Zhang L, Hui D (2022) A novel finishing approach for 3D printed inconel 718 by utilizing isotropic electrochemical etching. *J Mater Process Technol* 299:117356. <https://doi.org/10.1016/j.jmatprotec.2021.117356>
24. Chen X, Zhou J, Wang K, Xu Y (2021) Experimental research on single-pulse discharge crater morphology in SEAM. *Mater Manuf Process* 00:1–10. <https://doi.org/10.1080/10426914.2021.1954191>

Publisher's note Springer Nature remains neutral with regard to jurisdictional claims in published maps and institutional affiliations.

Springer Nature or its licensor holds exclusive rights to this article under a publishing agreement with the author(s) or other rightsholder(s); author self-archiving of the accepted manuscript version of this article is solely governed by the terms of such publishing agreement and applicable law.